Electronic Supplementary Information (ESI) for:

Activation of patternable ceramics for hydrogen evolution reaction using Molybdenum-based fillers

Quentin Hanniet[a], Zakaria Anfar[a], Hippolyte Dory[a], Sylvie Calas-Etienne[b], Pascal Etienne[b], Valérie Flaud[c], Jérôme Castellon[d], Benoit Charlot[d], Philippe Miele[a], Damien Voiry[a] and Chrystelle Salameh*[a]

Affiliations :

[a.] *Institut Européen des Membranes, IEM, UMR 5635, Univ Montpellier, CNRS, ENSCM, 34095 Montpellier Cedex 5, France.*
[b.] *Laboratoire Charles Coulomb (L2C), University of Montpellier, CNRS, Montpellier 34090, France.*
[c.] *Institut Charles Gerhardt, ICGM, UMR 5253, University of Montpellier, ENSCM, CNRS, 34095, Montpellier Cedex 5, France*
[d.] *Institut d'Electronique et des Systèmes (IES), UMR 5214, Université de Montpellier, CNRS, Montpellier 34090, Cedex 5, France*

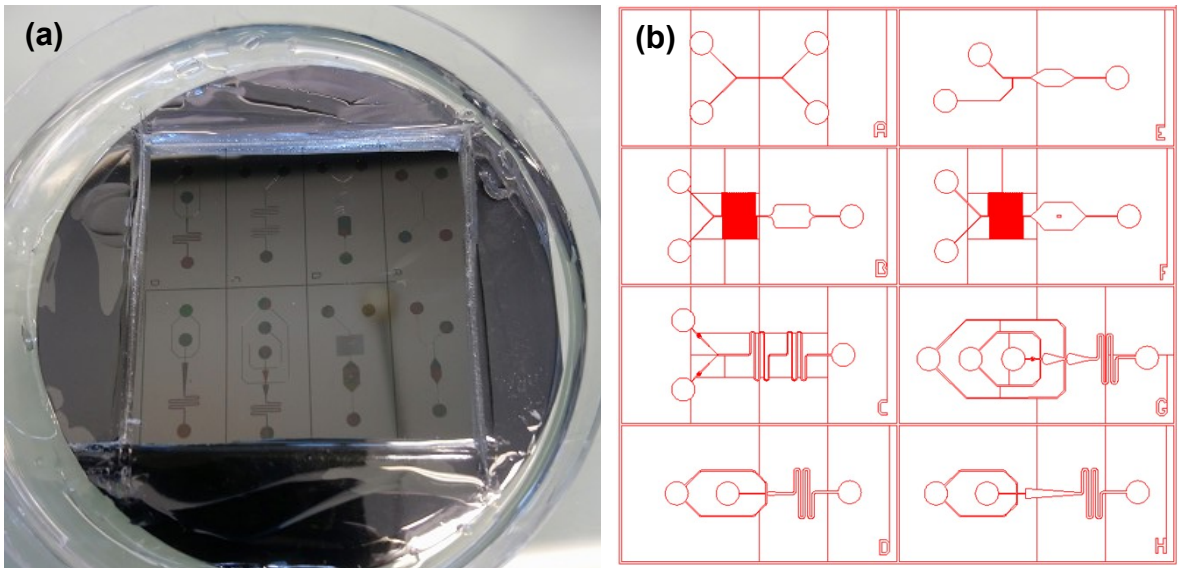

Fig. S1: (a) SU-8 masters prepared from (b) CAD layout.

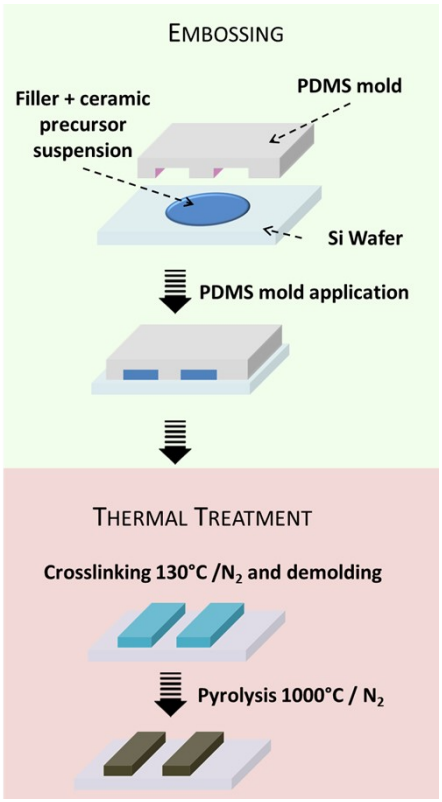

Fig. S2: Soft-lithography process for the preparation of ceramic/filler micropatterns. PVZ/filler suspensions were prepared using a Speedmixer, DAC 150.1 FV (1600 rpm for 2 min) and a few droplets were shaped using a PDMS mold. The micropattern was crosslinked at 200°C for 5h under N_2 and pyrolyzed, after demolding, at 1000°C for 2h.

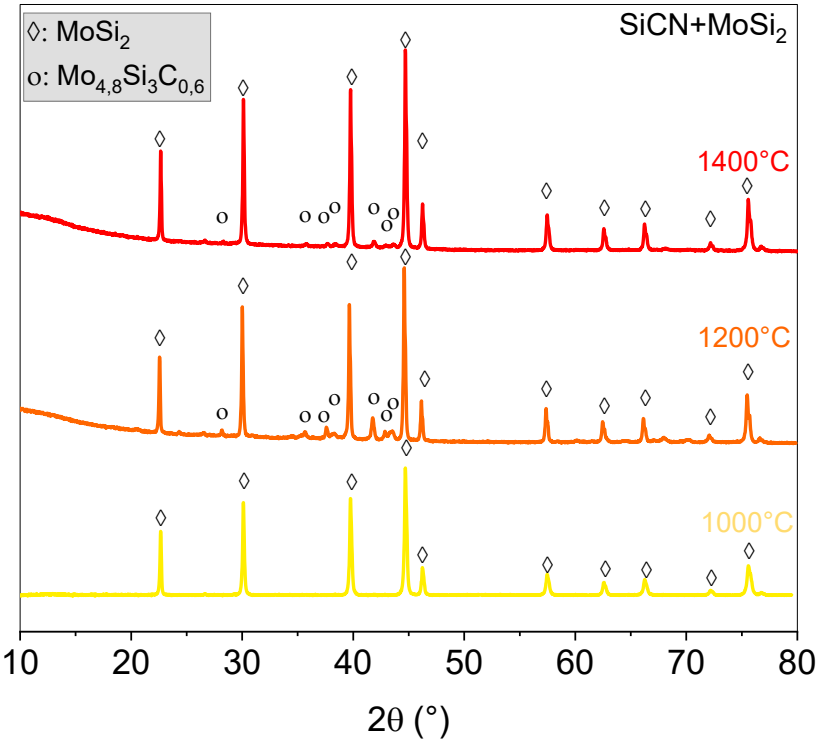

Fig. S3: XRD diffractograms of SiCN/$MoSi_2$ composite annealed at temperatures ranging between 1000 and 1400°C.

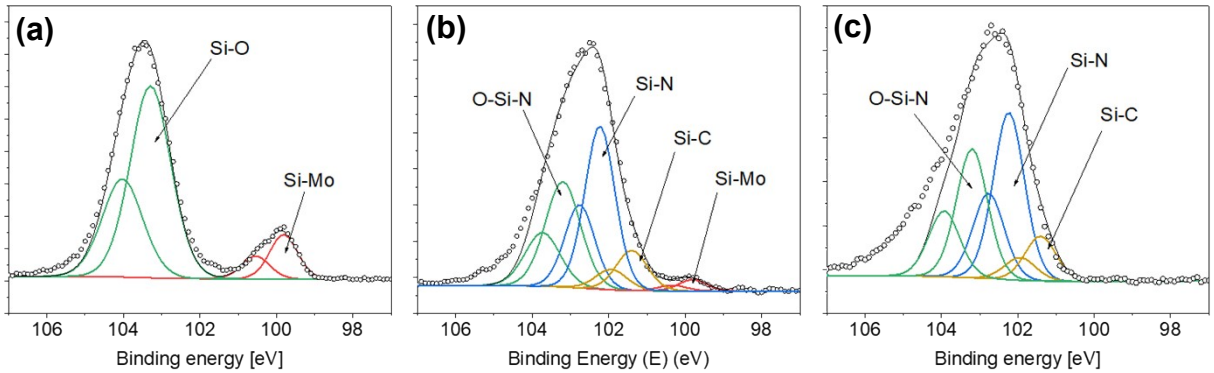

Fig. S4: XPS Si2p peaks recorded for (a) pristine $MoSi_2$, (b) SiCN/$MoSi_2$/MoS_2 and (c) SiCN/MoS_2 samples.

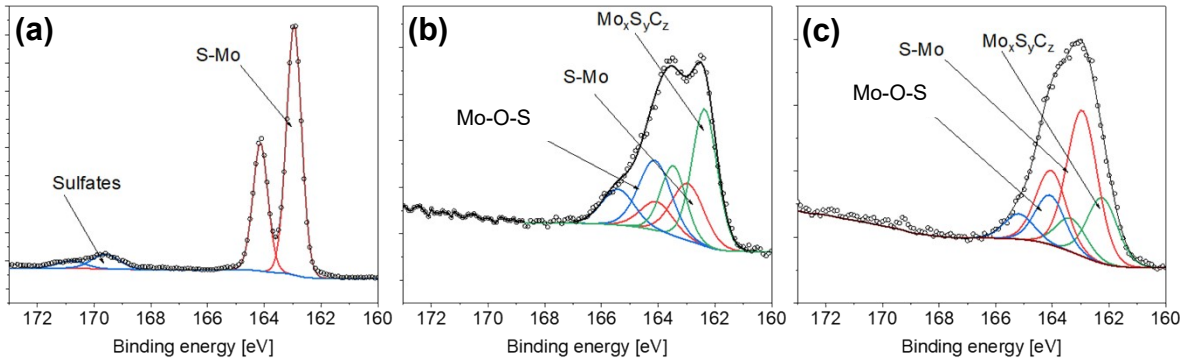

Fig. S5: XPS S2p peaks recorded for (a) pristine MoS_2, (b) SiCN/MoS_2 and (c) SiCN/$MoSi_2$/MoS_2 samples.

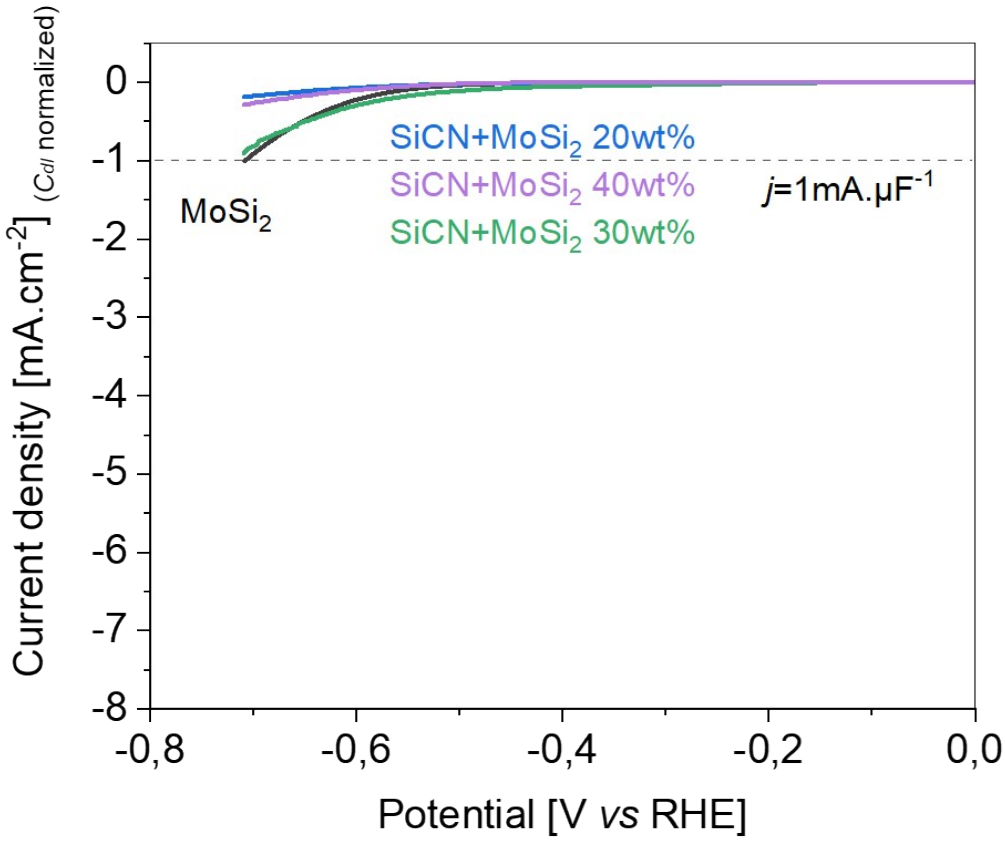

Fig. S6: CV curves of SiCN/$MoSi_2$ composites prepared with filler loading of 20 (blue), 30 (green) and 40 wt% (purple) along with pristine $MoSi_2$ (black).

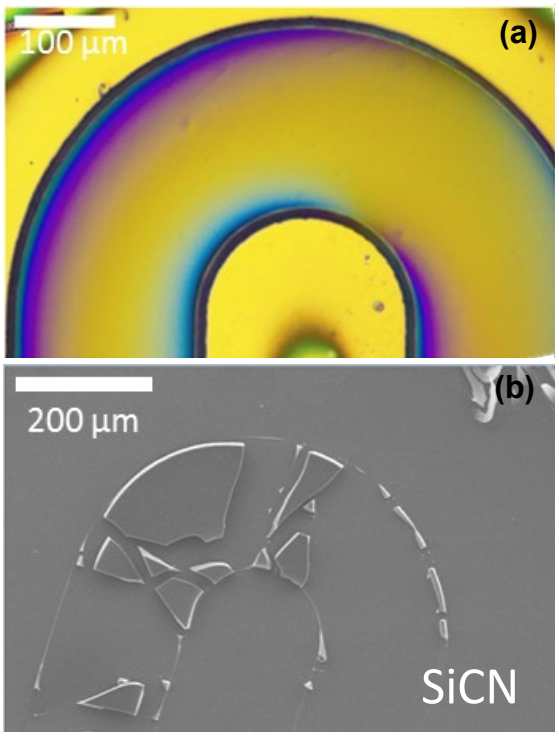

Fig. S7: Micrography of micropattern prepared from pure PVZ (a) before pyrolysis and (b) after pyrolysis.

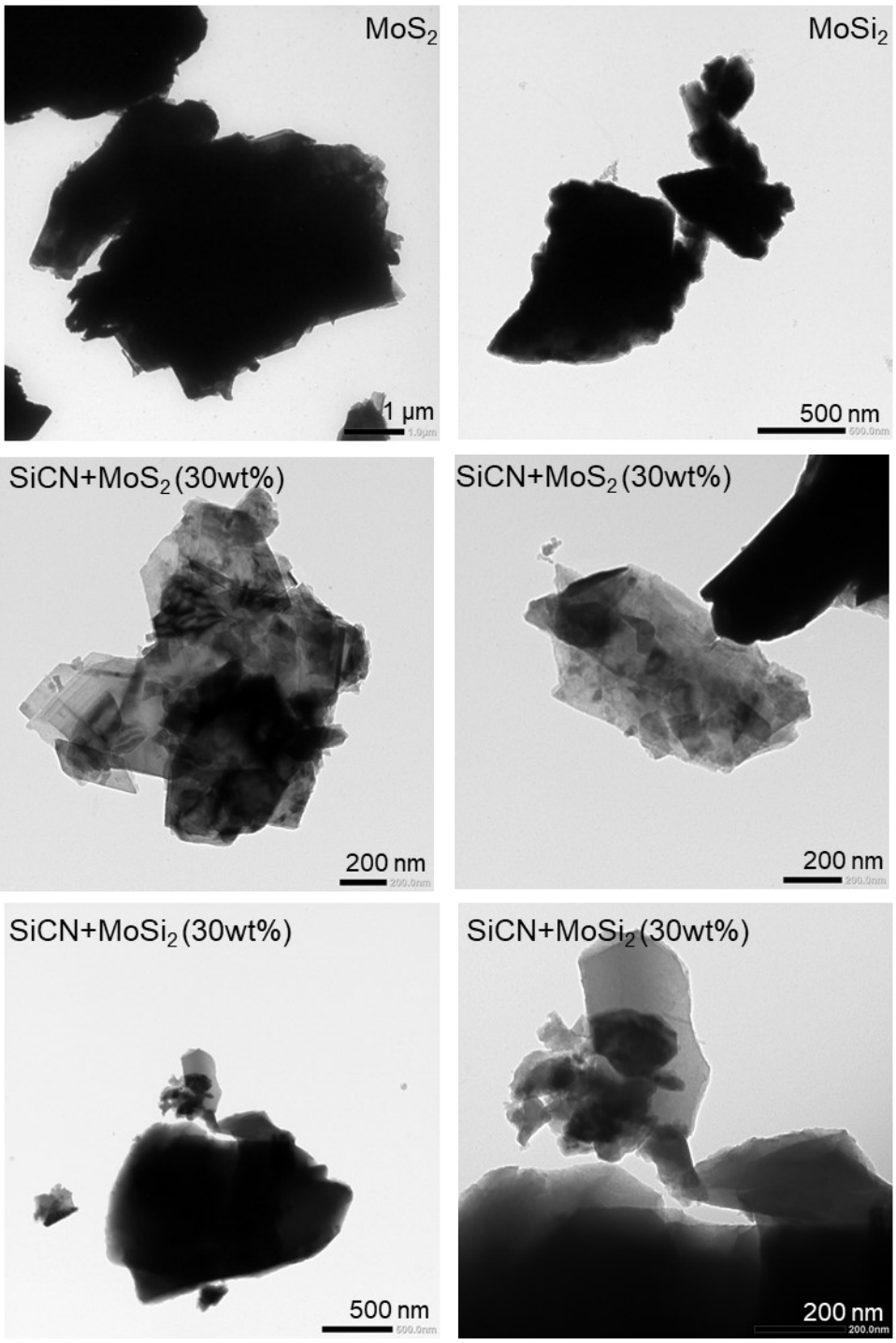

Fig. S8: TEM images of bulk MoS_2, $MoSi_2$, and the composites SiCN+MoS_2 30wt%, SiCN+$MoSi_2$ 30wt%. The materials were prepared by first dispersing 1 mg of sample in 20 mL of deionized water, followed by sonication for 20 minutes to ensure a uniform suspension. After sonication, 10 µL of the material suspension was drop-cast onto copper TEM grids coated with a carbon film. The TEM imaging was carried out using a JEOL 1400 microscope equipped with a 4-emission gun, operating at an accelerating voltage of 120 kV.

Figure S8 presents the TEM images of the bulk Mo-based additives, namely MoS_2 and $MoSi_2$, as well as the SiCN composites with 30 wt% MoS_2 and 30 wt% $MoSi_2$. This specific ratio was

chosen for the composites due to its optimal HER activity among all the ratios tested. As expected, the TEM images clearly show the two-dimensional nanosheet structure of bulk MoS_2 and the platelet-like morphology of bulk $MoSi_2$. Notably, the SiCN + 30 wt% MoS_2 composite retained the characteristic nanosheet structure, indicating that the ceramic matrix did not disrupt the 2D structure of MoS_2. Similarly, the SiCN + 30 wt% $MoSi_2$ composite preserved the platelet-like aspect of $MoSi_2$. These observations demonstrate that our approach successfully maintains the microstructural properties of 2D and 2D-like materials, thereby synergistically imparting their properties to the ceramic matrix.

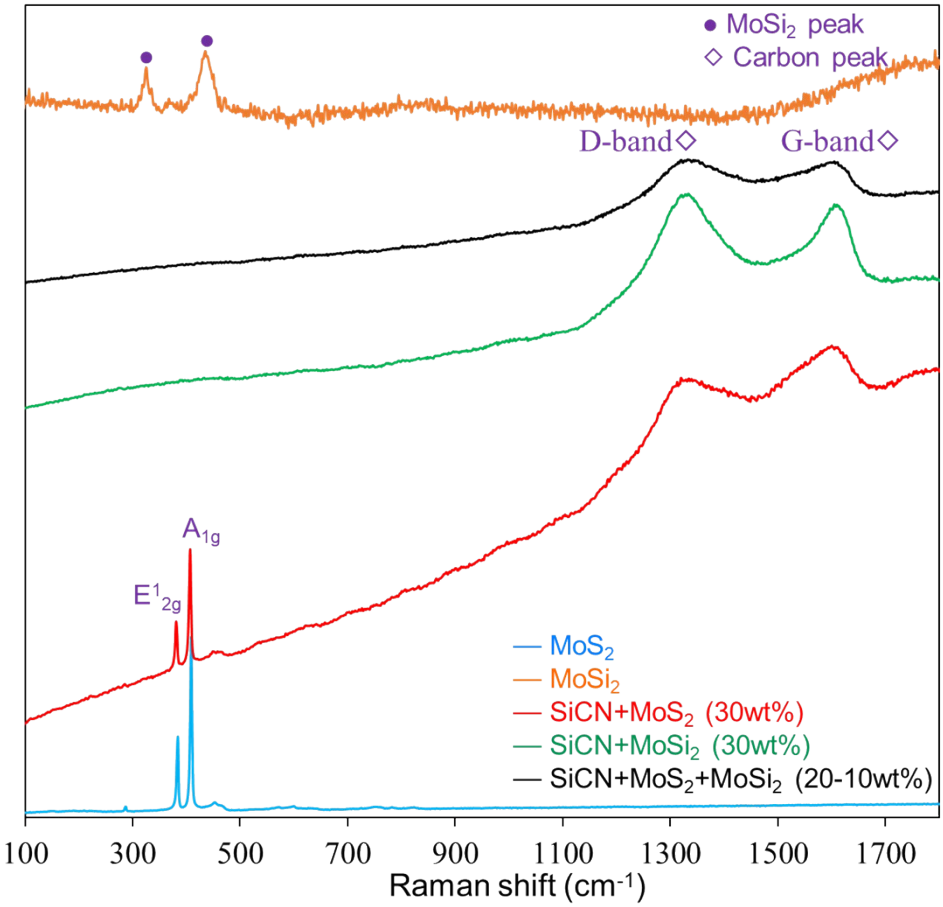

Fig. S9: Raman spectra of bulk MoS_2, $MoSi_2$, and the composites SiCN+MoS_2 30wt%, SiCN+$MoSi_2$ 30wt% and SiCN+MoS_2+$MoSi_2$ (20-10wt%). Raman spectroscopy was carried out using WITec alpha 300 confocal Raman microscope, 532 nm excitation wavelength. Condition: 1% of laser intensity and 600 accumulations (1 second step).

Fig. S9 shows the Raman spectra of bulk MoS_2, $MoSi_2$, and the composites SiCN+MoS_2 30wt%, SiCN+$MoSi_2$ 30wt% and SiCN+MoS_2+$MoSi_2$ (20-10wt%).These specific ratios were

selected due to their high HER activity. Distinct Raman shifts corresponding to $MoSi_2$ and MoS_2 confirm the crystalline structure of these materials. The Raman spectra of all three SiCN-based composites exhibit the G and D peaks, indicative of graphitic and disordered carbon phases that are observed in SiCN ceramics pyrolyzed at 1000°C. Notably, the SiCN + 30 wt% MoS_2 composite retained the microstructure of MoS_2, as evidenced by the preserved A_{1g} and E^1_{2g} Raman modes.

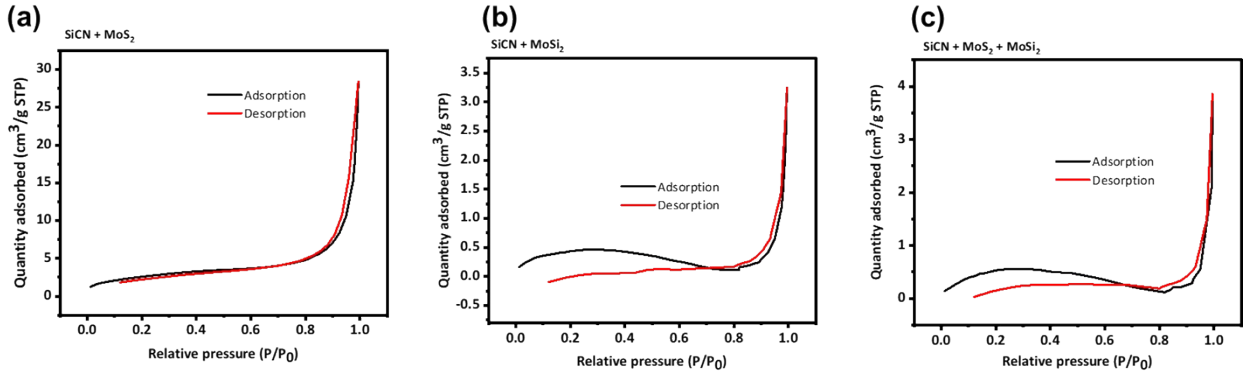

Fig. S10: N_2 adsorption isotherms for representative composites (a) SiCN+MoS_2 30wt%, (b) SiCN+$MoSi_2$ 30wt% and (c) SiCN+MoS_2+$MoSi_2$ 20-10wt%. N_2 adsorption was performed at −196 °C using an ASAP 2020 V4.04 (V4.04 H) micromeritics equipment. The samples were preheated at 200°C for 24 h under vacuum before the measurements.

The ceramic-based materials we synthesized were not initially expected to exhibit significant micro- or mesoporosity, as the additives used (MoS_2 and $MoSi_2$) were in powder bulk form. However, micro- and mesoporous polymer-derived ceramics (PDCs) with varied pore geometries, microstructures, and specific surface areas can be generated through the thermolysis of preceramic polymers. This process involves the decomposition of organic groups and the release of gaseous species, potentially inducing intrinsic porosity in the resulting ceramic products. Despite this potential, our BET measurements **(Fig.S10)** showed relatively low specific surface areas (BET SSA: 9.67 m^2/g for SiCN + MoS_2, 1.62 m2/g for SiCN + $MoSi_2$, and 2.26 m^2/g for SiCN + MoS_2+$MoSi_2$). The presence of hysteresis loops in all isotherms suggests capillary condensation, indicative of mesoporous structures with differing pore sizes and distributions. Notably, the SiCN + $MoSi_2$ sample may contain larger mesopores or even macropores, while the SiCN + MoS_2 sample appears to exhibit a more uniform mesoporosity.

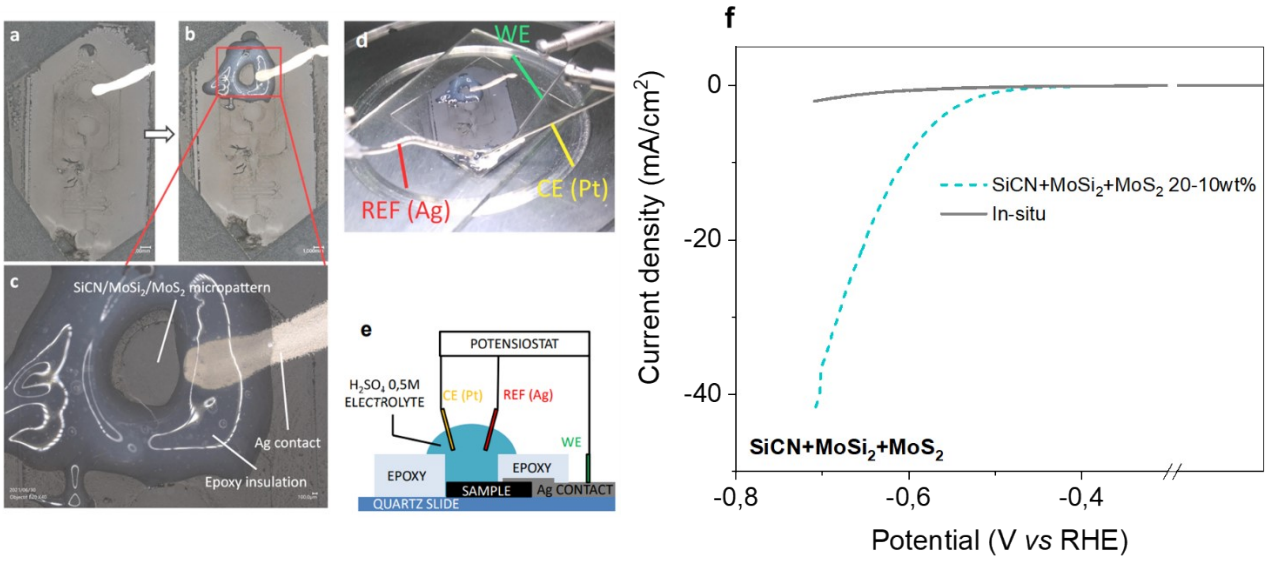

Fig. S11: (a-e) Preparation of SiCN/$MoSi_2$/MoS_2 micropattern for in-situ HER test (f).

We conducted real-time operational tests on the micro-devices and have included photographs and polarization curves from these experiments in the supplementary materials. Fig. S11 describes the preparation process of the micropattern for electrocatalytic measurements. A thin film of silver lacquer was used to create an electrical contact on the SiCN/$MoSi_2$/MoS_2 micropattern, connecting it to the working electrode. To prevent short-circuiting, the silver contact was sealed with epoxy resin. The electrocatalytic tests were conducted using a probe station equipped with micro-positioners connected to a potentiostat, as illustrated in Fig. S11d. The experiments were performed by placing a drop of 0.5M H_2SO_4 electrolyte solution on the micropattern, which was surrounded by epoxy to confine the liquid. The working electrode contact was maintained via the silver lacquer, while a platinum counter electrode and an Ag pseudo-reference electrode were immersed in the electrolyte drop. This configuration effectively recreated a three-electrode setup connected to a potentiostat, as depicted in Figure S11e.

Despite these efforts, we were unable to observe significant HER activity *in situ* (See Fig S11f). We attribute this limitation to the composite material's restricted electronic conductivity. While $MoSi_2$ was incorporated to enhance conductivity, as shown in Figure 4.d, the improvement was insufficient to support the current density needed for effective HER under real-time conditions. Additionally, the limited amount of conductive fillers used in the sample, due to poor colloidal dispersion, likely exacerbated this issue.